CHAPTER IV
PROGRAM TESTING

The developed program was applied to four representative problems, which involve in chemical engineering applications. The description for each particular problem is shown in Table 4.1.

Table 4.1 Test problem descriptions.

Problem	Coor - dinate	Steady state	Irregular geometry	Finite-difference applicable	Exact solution available
Heat conduction in finite slab: TP1	x, y or r, z	Yes	No	Yes	Yes
Turbine blade analysis: TP2	x, y	Yes	Yes	Yes	No
Slug flow analysis: TP3	r, z	Yes	Yes	No	No
Aeration pond analysis: TP4	x, y	No	Yes	No	No

4.1 Problem TP1: Heat Conduction in Finite Slab

4.1.1 Problem Definition

Heat transfer process is extremely important in chemical engineering field. It can be roughly classified into conduction, convection, and radiation. Heat conduction occurs with the existing of temperature gradient in any materials, solid or even liquid. The constitutive equation of heat conduction follows Fourier's law,

$$q = -k\nabla T, \qquad (4.1)$$

which states that heat flux by conduction is proportional to the temperature gradient. This expression is usually implemented to perform heat balance equations. For a simple case of two-dimensional steady state heat conduction,

$$k\frac{\partial^2 T}{\partial x^2} + k\frac{\partial^2 T}{\partial y^2} + G = 0, \tag{4.2}$$

and corresponding to that in axisymmetric cylindrical coordinate,

$$k\frac{1}{r}\frac{\partial T}{\partial r}\left(\frac{r\partial T}{\partial r}\right) + k\frac{\partial^2 T}{\partial z^2} + G = 0. \tag{4.3}$$

Here, first test problems, governing these two equations, were set up. Simple examples of heat conduction in a finite slab in both rectangular and cylindrical coordinates were examined. These two systems are simple adequately to reach analytical solutions. Thus, the temperature distributions throughout material can be solved both numerically and analytically. The solutions were finally discussed. The test systems are shown in Figure 4.1.

Heat conduction coefficient and heat generation throughout the material are values of 0.1 W/m K and 1000 W, respectively. The length (L) and radius of cylinder equal to 0.24 m. Slab is insulated at left surface (x = 0) and another boundary at x = L hold at temperature of 25 ^{o}C (Dirichlet type boundary condition). Convective boundary condition (mixed type) is also applied to the same systems, which, in tern, have heat convection coefficient (h) and surrounding temperature (Ts) of 25 W/m^2 K and 25 ^{o}C, respectively. The temperature profile throughout the slab was determined by both analytical and numerical approaches.

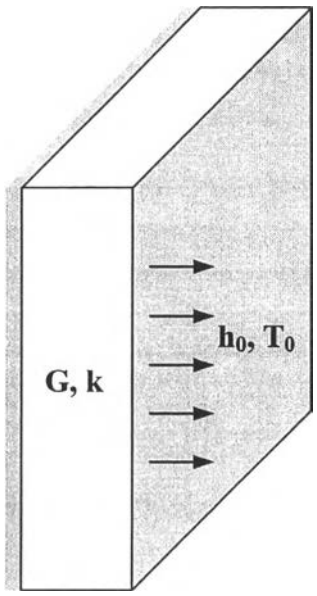

Figure 4.1 The slab system in test problem TP1.

4.1.2 Solution Strategy

4.1.2.1 Analytical solutions

The problems were reasonably considered as one dimension. So, the governing equations are reduced to,

$$k\frac{\partial^2 T}{\partial x^2} + G = 0, \tag{4.4}$$

$$\frac{1}{r}\frac{\partial}{\partial r}\left(kr\frac{\partial T}{\partial r}\right) + G = 0, \tag{4.5}$$

for rectangular and cylindrical coordinates, respectively. The exact solutions can be found by double integration these two equations. The solutions of the Dirichlet boundary type problems are:

$$T(x) = T_L + \frac{G}{2k}\left(L^2 - x^2\right), \tag{4.6}$$

$$T(r) = T_R + \frac{G}{4k}\left(R^2 - r^2\right). \tag{4.7}$$

For convective boundary, T_L and T_R are equal to

$$T_L = T_s + \frac{GL}{h}, \tag{4.8}$$

$$T_R = T_s + \frac{GR}{2h}, \tag{4.9}$$

for rectangular and cylindrical coordinates respectively.

4.1.2.2 Approximate solutions

On the other hand, a suitable system meshing was made and input to develop finite element program for finding approximate solution. To compare the results, difference mesh patterns and refinement were also considered. Mesh patterns are shown in Figure 4.2.

4.1.3 Results

For different system with temperature distributions, the exact solutions and approximate results from the FEM program (with pattern A mesh generation) are shown in Tables 4.2 and 4.3. Table 4.4 also shows the approximate results from different mesh patterns (for the case of convective boundary problem of rectangular coordinate only).

The results exhibited very good agreement between the approximate and analytical solutions with very small errors. The slightly different results from different mesh generations were also observed.

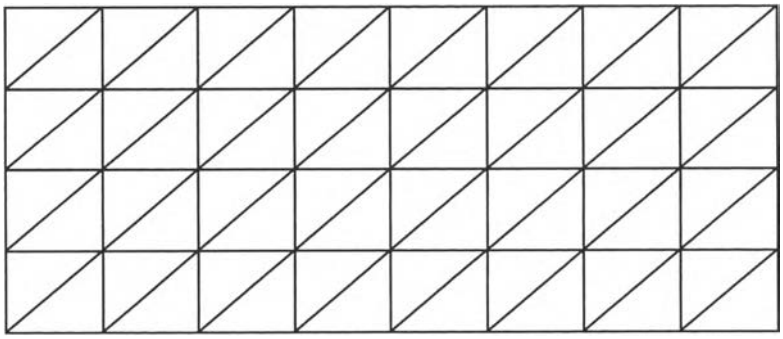

(a) Pattern A

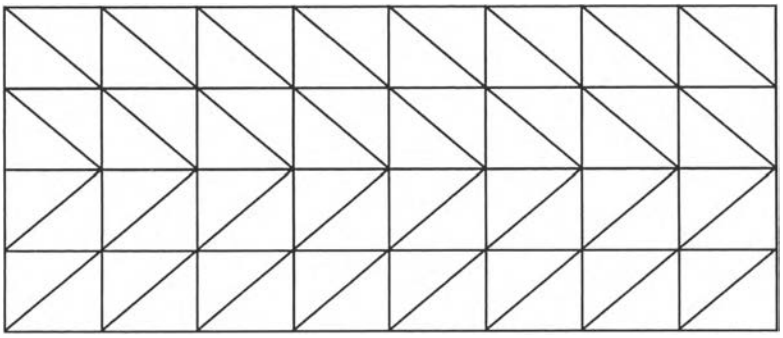

(b) Pattern B

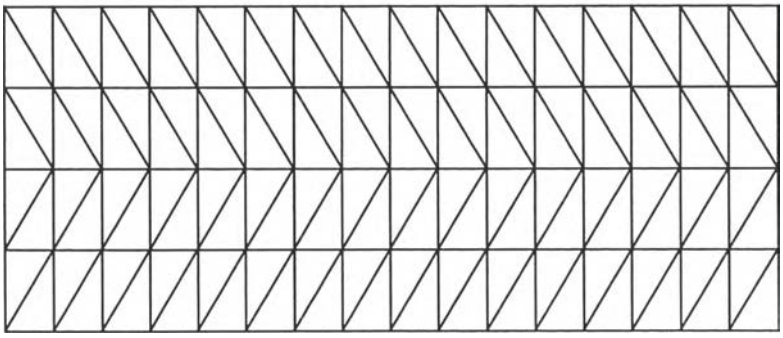

(c) Pattern C

Figure 4.2 Different mesh refinement patterns used in TP1 analysis.

Table 4.2 The numerical solutions to TP1 in rectangular coordinate.

x	For convective BC.		For Dirichlet type BC.	
	Approx.	Exact	Approx.	Exact
0.000	322.601	322.600	313.001	313.000
0.030	318.101	318.100	308.501	308.500
0.060	304.601	304.600	295.001	295.000
0.090	282.101	282.100	272.501	272.500
0.120	250.601	250.600	241.001	241.000
0.150	210.101	210.100	200.500	200.500
0.180	160.601	160.600	151.000	151.000
0.210	102.100	102.100	92.500	92.500
0.240	34.600	34.600	25.000	25.000

Table 4.3 The numerical solutions to TP1 in cylindrical coordinate.

r	For convective BC.		For Dirichlet type BC.	
	Approx.	Exact	Approx.	Exact
0.000	174.334	173.800	170.395	169.000
0.030	171.657	171.550	167.475	166.750
0.060	164.902	164.800	160.500	160.000
0.090	153.635	153.550	149.108	148.750
0.120	137.857	137.800	133.254	133.000
0.150	117.580	117.550	112.922	112.750
0.180	92.818	92.800	88.105	88.000
0.210	63.599	63.550	58.798	58.750
0.240	29.980	29.800	25.000	25.000

Table 4.4 The solutions to TP1 in rectangular coordinate with different mesh patterns (convective BC-type problems).

x	Solutions from different meshing			Exact Solution
	Pattern A	Pattern B	Pattern C	
0.000	322.601	322.601	322.601	322.600
0.100	318.101	318.101	318.101	318.100
0.200	304.601	304.601	304.600	304.600
0.300	282.101	282.100	282.100	282.100
0.400	250.601	250.600	250.600	250.600
0.500	210.101	210.100	210.100	210.100
0.180	160.601	160.600	160.600	160.600
0.210	102.100	102.100	102.100	102.100
0.240	34.600	34.600	34.600	34.600

4.2 Problem TP2:Turbine Blade Analysis

4.2.1 Problem Definition

Here, the problem is still not apart from heat conduction, but more applicable. The governing equation was analogous to Equation 4.2. A major objective in advancing gas turbine engine technologies is to increase the temperature limit associated with operation of the gas turbine blades. This limit determines the permissible turbine gas inlet temperature, which strongly influences overall system performance. In addition to fabricating blades from special, high temperature, high-strength superalloys, it is common to use internal cooling by machining flow channels within the blades and routing air through the channels. Here, simplification by approximating the blade as a rectangular solid in which rectangular channels are machined is made. The blade, which has a thermal conductivity of k = 25 W/m K, is 6 mm thick, and each channel has a 2 mm x 6 mm rectangular cross section, with a 4 mm spacing between adjoining channels as shown in Figure 4.3.

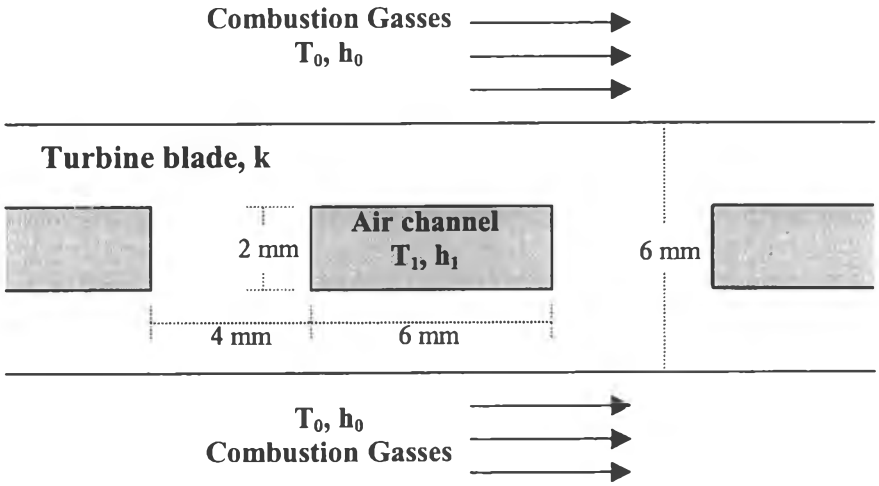

Figure 4.3 Turbine blade

Under operating conditions for which h_0 = 1000 W/m^{2}K, T_0 = 1700 K, h_1 = 200 W/m^{2}K, and T_1 =400 K, the temperature field in the turbine blade was determined via finite element and finite difference methods.

4.2.2 Solution Strategy

Symmetry of the blade shape allows the problem to be simplified. A new system, comprising two pseudo-insulated (Neumann type) and two convective (mixed type) boundaries, was adapted. System meshing and detail of node arrangement are shown in Figure 4.4.

4.2.3 Results

The numerical results for each node from the FEM program can be exhibited in Table 4.5, comparing to solution of finite difference method available in Incropera and DeWitt (1996). With the same number of discretized node, two solutions do not show a significant difference from each other.

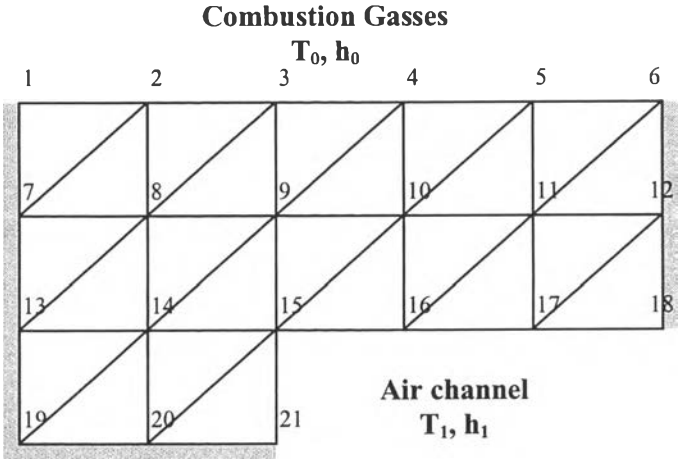

Figure 4.4 Mesh generation for system TP2.

Table 4.5 The temperature distribution in turbine blade.

Node	Temperature (K) at each node obtained from	
	FEM	FDM
1	1526.0	1526.0
2	1525.3	1525.3
3	1523.6	1523.6
4	1521.9	1521.9
5	1520.8	1520.8
6	1520.4	1520.5
7	1519.7	1519.7
8	1518.8	1518.8
9	1516.5	1516.5
10	1514.5	1514.5
11	1513.3	1513.3
12	1512.9	1512.9
13	1515.1	1515.1

Node	Temperature (K) at each node obtained from	
	FEM	FDM
14	1513.7	1513.7
15	1509.2	1509.2
16	1506.4	1506.4
17	1504.9	1505.0
18	1504.5	1504.5
19	1513.4	1513.4
20	1511.7	1511.7
21	1506.0	1506.0

For further analysis, graphical result from FEM program was considered. Temperature profile inside material of turbine blade system was exhibited in Figure 4.5. Figure 4.6 shows the system after reassembling other symmetric parts.

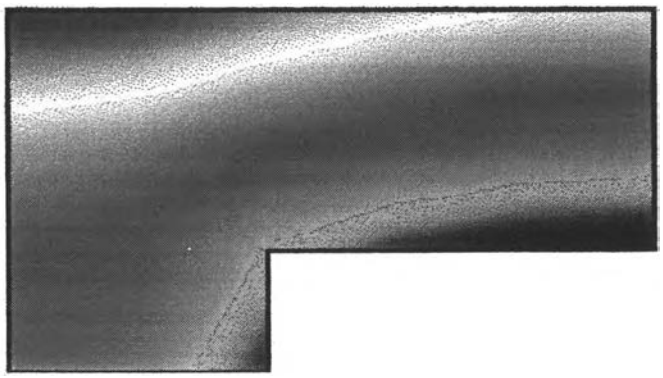

Figure 4.5 Graphical solution to problem TP2.

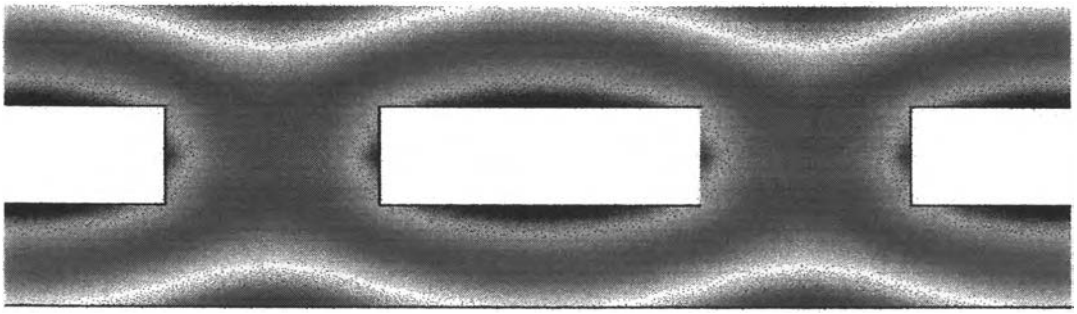

Figure 4.6 Temperature profile in turbine blade.

From the temperature profile of the blade exhibited in Figure 4.6, the red color represents a high temperature region in the material. On the other hand, the blue color represents a low temperature region, which concentrated at the inner side of the blade contacting with the cooling media cavities. This shade exhibition is useful for further analysis of the blade e.g., deformation or even failure of the blade etc.

4.3 Problem TP3: Slug Flow Analysis

4.3.1 Problem Definition

Two-phase flow in a vertical tube is an important phenomenon in petroleum and chemical engineering processes e.g., in evaporators and in simultaneous transport of oil and gas from wells. Several regimes of flow occur from bubble to slug, annular and mist flow, respectively. Slug flow is relatively important in term of analysis. In slug flow regime, gas bubbles coalesce together in form of gas slugs, while the liquid phase is still continuous as exhibited in Figure 4.1.

In slug flow analysis, rising velocity of slug is obtained (Nicklin *et al.*, 1962) as

$$u_s = 1.2\left(\frac{G+L}{A}\right) + c\sqrt{gD} \tag{4.10}$$

where G and L are gas and liquid volumetric flow rate, respectively, A is cross-sectional area of the pipe, and $c\sqrt{gD}$ is defined as slug velocity in stagnant liquid (or u_b) and c equal to 0.35, where g is gravitational acceleration, and D is pipe diameter.

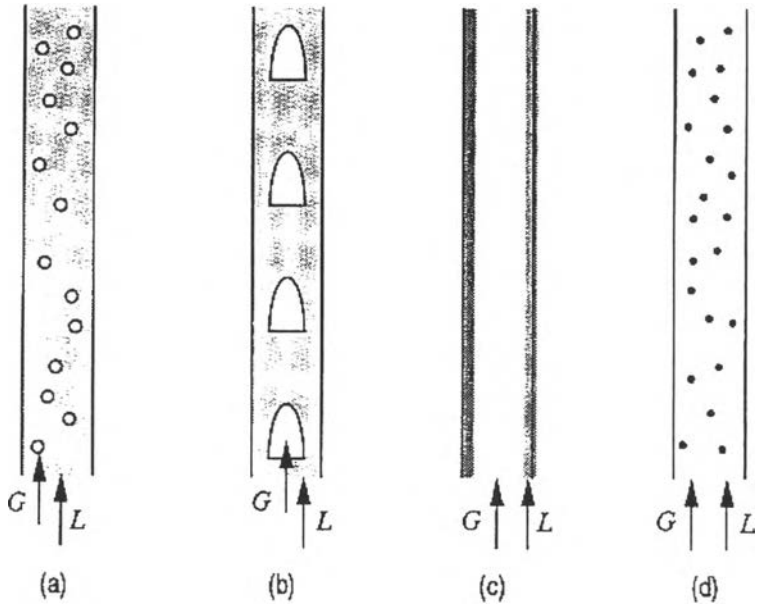

Figure 4.7 Four regimes of two-phase flow in vertical tube: (a) bubble, (b) slug, (c) annular, and (d) mist flow.

Further analysis is purposed by taking the Langrangian viewpoint of an observer travelling upward with slug. The resulting potential flow is governed in cylindrical coordinate known as Laplace's equation (Wilkes and La Valle, 1990)

$$\frac{\partial^2\phi}{\partial r^2} + \frac{1}{r}\frac{\partial\phi}{\partial r} + \frac{\partial^2\phi}{\partial z^2} = 0, \tag{4.11}$$

where ϕ is the potential function, and is such that the radial and axial velocity components of liquid around the gas slug are given by

$$u_r = -\frac{\partial \phi}{\partial r}, \tag{4.12}$$

$$u_a = -\frac{\partial \phi}{\partial z} \tag{4.13}$$

Solving these equations allows a velocity profile of liquid to be found and the result next can be represented in the form of equipotential lines outer the slug that well describe its behavior. Here, the proper shape of slug was also determined.

Figure 4.8 shows system meshing for the liquid around a gas slug. The tube radius, a, equal to 0.95 cm.

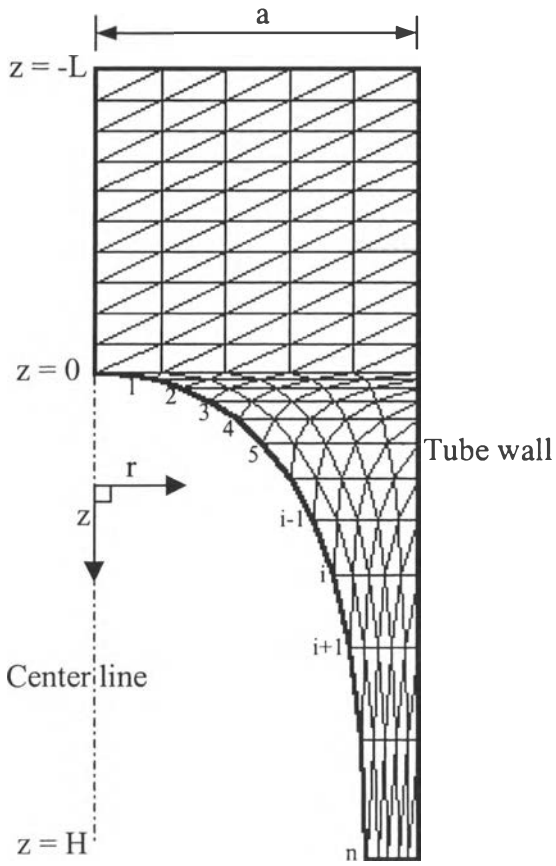

Figure 4.8 System meshing for the liquid around a gas slug.

4.3.2 Solution Strategy

After guessing the shape of slug, a systematic meshing was made and input to the FEM program. The potential distribution throughout the liquid was determined case by case. The tangential velocities v_i at the interface points were obtained by differentiating the computed values of ϕ in the direction of the interface. For example, at point i,

$$v_i = \frac{1}{2}\left(\frac{\phi_i - \phi_{i-1}}{s_{i,i-1}} + \frac{\phi_{i+1} - \phi_i}{s_{i+1,i}} \right), \qquad (4.14)$$

which s is the distance between two node points. These tangential velocities must satisfy Bernoulli's equation at all interface points (Wilkes and Bike, 1999),

$$v_i = \sqrt{2gz_i} \ . \qquad (4.15)$$

To accomplish the proper shape of slug, the exit potential and redial coordinates of all interface points were varied until their velocities satisfy Bernoulli criteria. The rise velocity and constant, c, were consequently determined.

4.3.3 Results

Table 4.6 represents the rise velocity and constant, c, from approximation compared to theory values. The results show very small difference between two values. Table 4.7 represents interfacial points coordinates of proper shape of slug and comparison between their velocities from approximations using the FEM program and theory values. Two solutions also show very good agreement with less than one percent relative error for every interface point.

Table 4.6 Rise velocity determined from approximation.

	Approx. value	Theory value	% Error
Rise velocity, u_b (cm/s)	15.096	15.100	0.026
Constant, C	0.349	0.350	0.286

Table 4.7 Coordinates and velocities at all interface points of proper slug shape.

r cm.	z cm.	V (approx.) cm/s	V (Bernoulli) cm/s	% Error
0.000	0.00	0.00	0.00	0.00
0.174	0.02	6.23	6.26	0.06
0.254	0.05	10.00	9.91	0.10
0.333	0.09	13.32	13.29	0.13
0.417	0.15	17.23	17.16	0.17
0.493	0.23	21.27	21.24	0.21
0.578	0.34	25.77	25.83	0.26
0.648	0.48	30.72	30.69	0.31
0.708	0.66	35.96	35.99	0.36
0.750	0.90	42.14	42.02	0.42
0.787	1.20	48.66	48.52	0.49

Figure 4.9 exhibits the proper shape of the slug obtained from FEM program compared to the experimental results. It shows the validity of the numerical solutions.

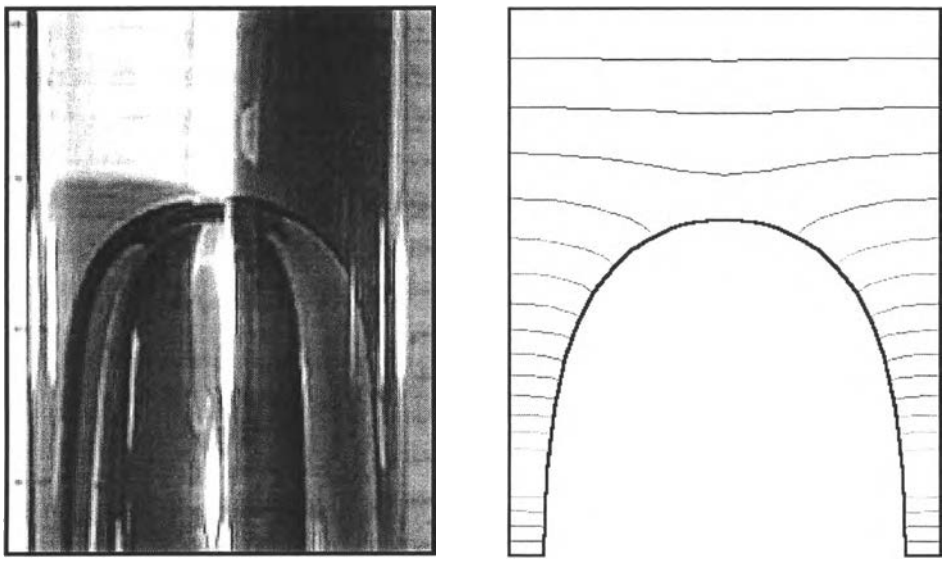

(a) actual slug (b) slug from FEM analysis

Figure 4.9 The proper shape of slug obtained from experiment and approximation via FEM program.

4.4 Problem TP3: Aeration Pond Analysis

4.4.1 Problem Definition

This problem deals with mass transfer phenomenon. The unsteady state mass diffusion equation in two dimensions was considered,

$$D_L\left(\frac{\partial^2 C}{\partial x^2}+\frac{\partial^2 C}{\partial y^2}\right)=\frac{\partial C}{\partial t} \qquad (4.16)$$

where D_L and C are mass diffusivity and concentration of dissolved species in media.

The minimum amount of chemicals dissolved in water as generally known is controlled by environmental regulations. Wastewaters must be treated before releasing to natural resources. Oxygen is one of major parameters to be accounted. Aeration pond is an alternative to solve this important problem in many industries. Here, test problem was set up. Figure 4.10 exhibits the wastewater pond, which was designed to use two aerators. The concentration of oxygen was assumed

to be saturated within the aerator-work radii. The pond edge is the Neumann type boundary. The system was also assumed to be two dimensions, which was very rough assumption. The concentration profile of oxygen throughout the pond was then determined with respect to time.

4.4.2 Solution Strategy

A suitable system meshing was created (Figure 4.10) and input to the FEM program. The concentration profile of oxygen throughout the pond was then solved.

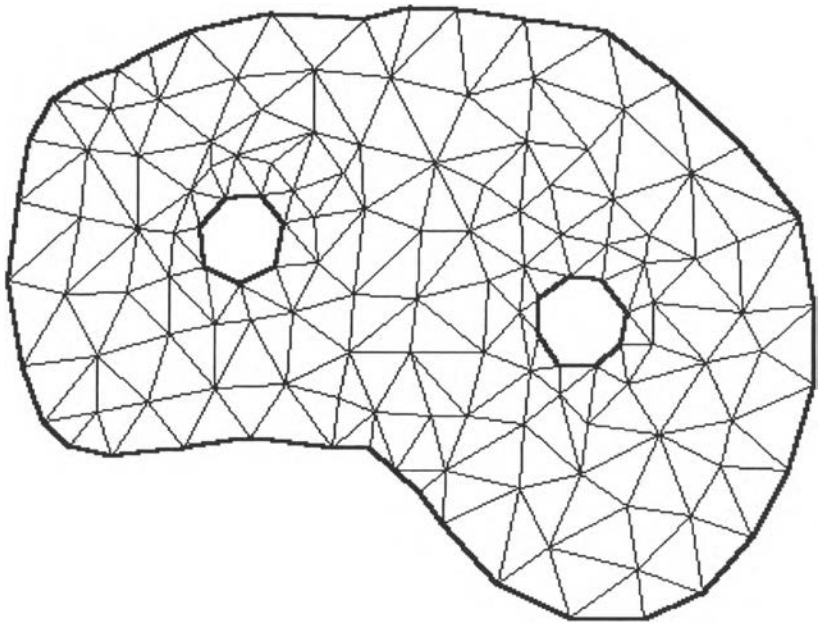

Figure 4.10 Aeration pond system and mesh generation in TP4

4.4.3 Results

The result of the FEM program was exhibited in the form of equal-concentration lines shown in Figure 4.11. The red shade represents the higher concentration region. The concentration of oxygen throughout the pond was increased with increasing time. The program showed the interface that describes the system very well. This analysis is very useful for designing the location of aerators or even aeration time needed to reach desired oxygen concentration.

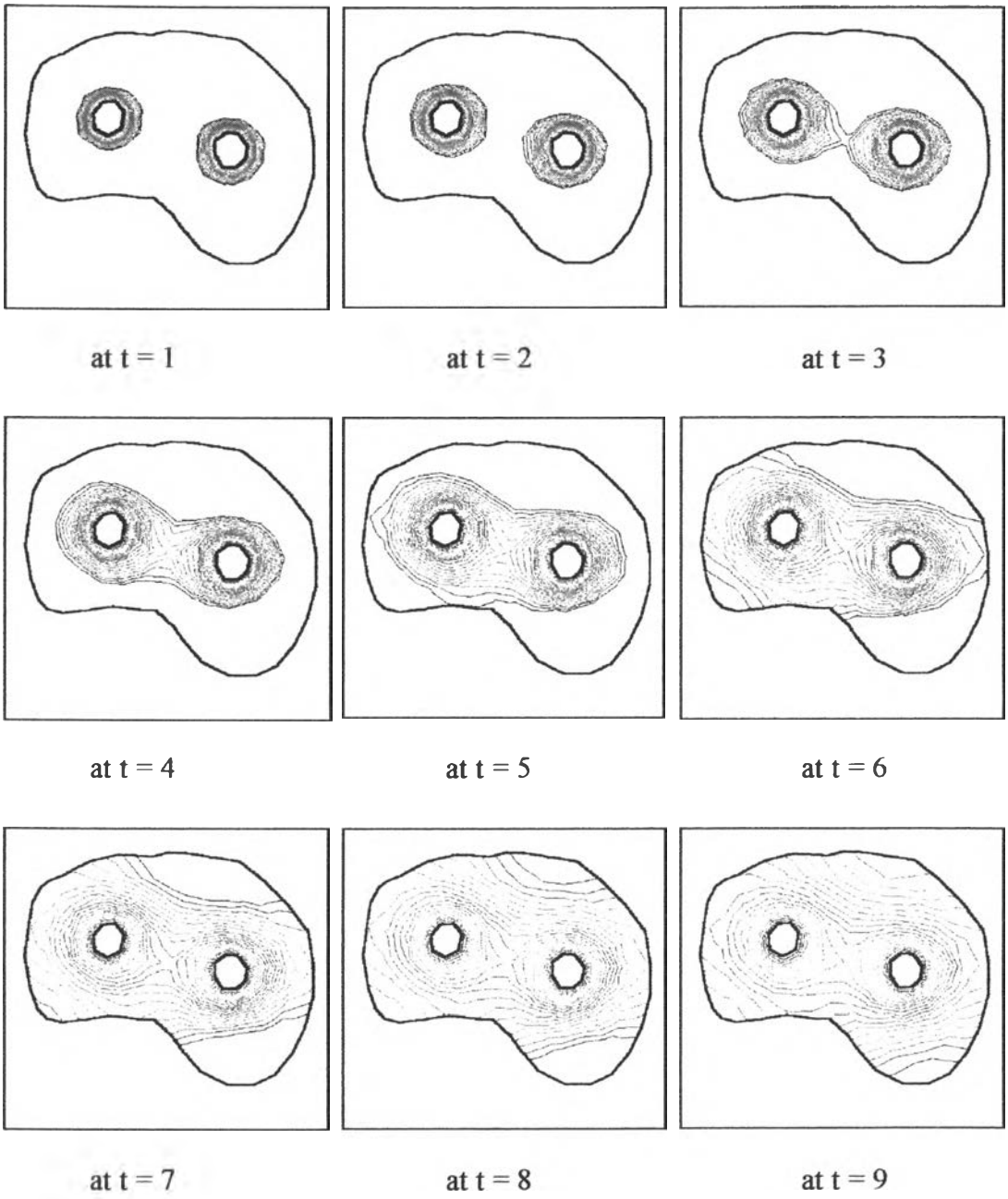

Figure 4.11 Concentration profile of oxygen in aerated pond.